Enhancement in Kinetics of the Oxygen Reduction Reaction on a Nitrogen-Doped Carbon Catalyst by Introduction of Iron via Electrochemical Methods

ARTICLE *in* LANGMUIR · APRIL 2015

Impact Factor: 4.46 · DOI: 10.1021/acs.langmuir.5b00310 · Source: PubMed

Langmuir

Article

pubs.acs.org/Langmuir

Enhancement in Kinetics of the Oxygen Reduction Reaction on a Nitrogen-Doped Carbon Catalyst by Introduction of Iron via Electrochemical Methods

Jiajia Wu,[†,‡] Da Zhang,[†,§] Hideharu Niwa,[∥,⊥] Yoshihisa Harada,[∥,⊥] Masaharu Oshima,[⊥] Hironori Ofuchi,[#] Yuta Nabae,[¶] Takeyoshi Okajima,[†] and Takeo Ohsaka*[,†]

[†]Department of Electronic Chemistry, Interdisciplinary Graduate School of Science and Engineering, Tokyo Institute of Technology, 4259 Nagatsuta, Yokohama, Kanagawa 226-8502, Japan

[‡]Key Laboratory of Marine Environmental Corrosion and Biofouling, Chinese Academy of Sciences, 7 Nanhai Road, Qingdao, Shandong 266071, People's Republic of China

[§]School of Environmental and Materials Engineering, Shanghai Second Polytechnic University, Jinhai Road 2360, Pudong New Area, Shanghai 201209, People's Republic of China

[∥]Institute for Solid State Physics, University of Tokyo, Kashiwanoha, Chiba 277-8581, Japan

[⊥]Synchrotron Radiation Research Organization, University of Tokyo, Sayo-cho, Hyogo 679-5198, Japan

[#]Japan Synchrotron Radiation Research Institute, Sayo-cho, Hyogo 679-5198, Japan

[¶]Department of Organic and Polymeric Materials, Graduate School of Science and Engineering, Tokyo Institute of Technology, Ookayama, Tokyo 152-8552, Japan

Supporting Information

ABSTRACT: The iron (Fe) electrodeposition−electrochemical dissolution has been employed on nitrogen-doped carbon material (P-PI) prepared via multi-step pyrolysis of a polyimide precursor to achieve the introduction of Fe species, and its influence on the oxygen reduction reaction (ORR) is investigated by cyclic and rotating ring-disk electrode voltammetry in 0.5 M H_2SO_4. After the electrochemical treatment, the overpotential and H_2O_2 production percentage of ORR on the P-PI are decreased and the number of electrons transferred is increased in the meanwhile. In combination with the results of X-ray absorption fine structure spectra, the presence of Fe−N_x sites (Fe ions coordinated by nitrogen) is believed to be responsible for the improved ORR performance. Further kinetic analysis indicates that a two-electron reduction of O_2 is predominant on the untreated P-PI with coexistence of a direct four-electron transformation of O_2 to H_2O, while the introduction of Fe species leads to a larger increase in the rate constant for the four-electron reduction than that for the two-electron process, being in good agreement with the view that Fe−N_x sites are active for four-electron ORR.

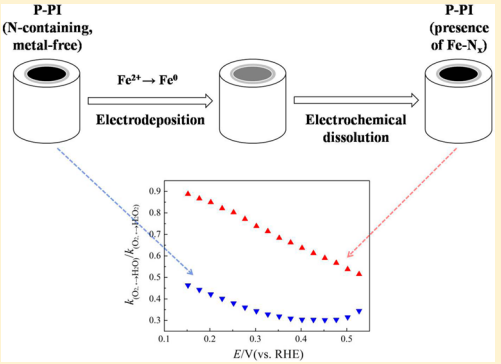

1. INTRODUCTION

Sluggish kinetics of the oxygen reduction reaction (ORR) at the cathode is a critical limit for the performance of polymer electrolyte membrane fuel cells (PEMFCs), which have attracted much attention as a clean energy source candidate in transportation, portable, and stationary applications. Platinum (Pt)-based materials have been commonly used as catalysts to promote ORR by their high activity, but the scarcity and high cost of Pt prevent the general commercialization of PEMFCs. In comparison to reducing the loading of Pt, the exploration of non-precious catalysts with good ORR performance is a better choice. Among those catalysts reported, nitrogen-doped carbon (NDC) materials have attracted intensive concern.

NDC materials can be divided into two categories: without or with transition metals. Most studies for the former are carried out in alkaline media, where some exhibit ORR catalytic activity approaching or higher than that of commercial Pt/C,[1−4] but these materials suffer low activity in acid media, probably because of relatively few active sites.[5,6] Luckily, the activity of metal-free NDC catalysts can be improved by the introduction of transition metals (typically Fe and Co), which is commonly accomplished by pyrolysis of the mixture in transition metal, nitrogen, and carbon sources,[7,8] or post-heat treatment of NDC materials together with transition metal precursors.[9,10] Although extensive studies have been conducted on metal-containing NDC catalysts, the role of transition metals in the enhancement of ORR activity is still in

Received: January 27, 2015
Revised: March 25, 2015
Published: April 22, 2015

DOI: 10.1021/acs.langmuir.5b00310
Langmuir 2015, 31, 5529−5536

controversy,[11] which is closely associated with complicated chemical and structural transformation during thermal treatment at high temperatures. For metal-free NDC catalysts, the ORR activity originates from the bonding between nitrogen and carbon, where high positive charge density on the adjacent carbon atoms is created by the relatively stronger electron affinity ability of nitrogen atoms.[12] While for metal-containing NDC catalysts, besides nitrogen−carbon sites, different states of metals are present, including metal ions coordinated by nitrogen ($M-N_x$) and nanoparticles of metal, metal oxide, or metal carbide. Some scientists insist that metals are key components of active sites, regardless of whether they are in the form of $M-N_x$ or nanoparticles.[13−15] On the other hand, others question the direct role of transition metals; namely, they believe that active sites are the same as those in metal-free NDC catalysts and metals facilitate the formation of nitrogen−carbon sites during heat treatment.[16−18] Therefore, if the incorporation of transition metals without great influence on microstructures of NDC catalysts can be achieved at low temperatures, it will shed light on the dispute about the role of transition metals. In this study, for the first time, we attempt to create Fe-containing catalysts by the electrochemical treatment of metal-free NDC material (P-PI) synthesized via multi-step pyrolysis of a polyimide precursor. The present results demonstrate that the ORR performance is improved by the electrochemical treatment carried out at room temperature, which is closely related to the presence of $Fe-N_x$ sites.

Rotating ring-disk electrode (RRDE) voltammetry is an effective tool for the investigation of ORR kinetics. Most papers are focused on H_2O_2 production percentage ($\chi_{H_2O_2}$), the number of electrons transferred (n), Tafel slope, and kinetic current density obtained from RRDE voltammograms.[19,20] Although these data give useful information on kinetics, there is still some uncertainty in the ORR process. For example, a value of 3 for n means the coexistence of two- and four-electron ORR, but there are two possibilities: parallel ($k_1 = k_2$ and $k_3 = 0$) and serial ($k_2 = 2k_3$ and $k_1 = 0$) pathways shown in Scheme 1. Consequently, it is better to obtain the values of k_1, k_2, and k_3

Scheme 1. ORR Model Proposed by Damjanovic et al.[21] [a]

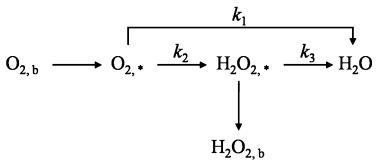

[a]Subscripts ∗ and b denote the species in the vicinity of the electrode surface and in the bulk solution, respectively.

to identify the mechanism. In this study, we have compared the values of k for ORR on the P-PI catalysts with and without the introduction of Fe, and the results indicate that k_1 is largely promoted by the presence of $Fe-N_x$ species.

2. EXPERIMENTAL SECTION

2.1. Preparation of P-PI. P-PI was prepared by a similar method reported in our recent paper without the addition of $Fe(C_5H_7O_2)_3$,[22] which can be divided into two steps. First, polyimide fine particles were synthesized by curing of poly(amic) acid that was obtained by the reaction of pyromellitic acid dianhydride with 4,4′-oxidianiline in acetone. Second, multi-step pyrolysis was employed on polyimide, including heat treatment at 600 °C for 5 h under N_2 flow, 800 °C for 1 h under NH_3, and 1000 °C for another 1 h under NH_3.

P-PI as-synthesized gives a morphology of fine particles with a size of around 100 nm, and the atomic contents of carbon, hydrogen, nitrogen, and oxygen are 65.94, 17.04, 4.61, and 12.41%, respectively. According to the results of X-ray photoelectron spectroscopy (XPS; see Figure S1A of the Supporting Information), four types of nitrogen are present in P-PI, with levels of 32.0, 31.2, 28.8, and 8.0% for pyridinic, pyrrolic, quaternary nitrogen, and nitrogen oxide, respectively.

2.2. Electrochemical Treatment of Modified Glassy Carbon (GC) Electrodes. A RRDE with a GC disk (diameter of 6 mm) and a Pt ring was used, and the modification of the disk electrode with P-PI was conducted by physical casting. Before modification, the electrode was polished with alumina slurries and washed in Milli-Q water by ultrasonication. P-PI ink was prepared by adding 5 mg of powder into a tube with a mixture of 50 μL of Nafion solution (5 wt %), 150 μL of ethanol, and 150 μL of Milli-Q water and then ultrasonication in ice-cold water for 2 h. A total of 4 μL of uniform ink was cast on the GC surface with a micropipette, and the loading density of P-PI was 200 μg cm^{-2}. The thus-modified electrode was dried completely at room temperature and designated as the P-PI/GC electrode. The multi-wall carbon nanotubes modified GC (MWCNTs/GC) electrode was also prepared in the same way for comparison.

The electrochemical treatment consists of two steps: electrodeposition and electrochemical dissolution of Fe. Fe electrodeposition on the P-PI/GC electrode was accomplished by cyclic voltammetry, which has been reported by several groups.[23,24] Here, the potential imposed on the P-PI/GC electrode was from open-circuit potential (ca. 0.46 V) to −0.873 V and then back to ca. −0.573 V, where the current is close to zero in Ar-saturated 0.5 M Na_2SO_4 containing 0.1 M $FeSO_4$ with a scan rate of 5 mV s^{-1}. After washing with Milli-Q water, Fe as-deposited was dissolved electrochemically by potential scanning in Ar-saturated 0.5 M H_2SO_4 for 10 cycles in the range between 0.077 and 1.127 V (50 mV s^{-1}). All electrochemical experiments in this study were performed on a CHI 760D electrochemical station with a three-electrode system, in which Ag/AgCl (KCl saturated) and Pt wire or carbon plate (the case for ORR measurements) were used as reference and counter electrodes, respectively. All of the potentials are referred to a reversible hydrogen electrode (RHE) by conversion from Ag/AgCl (KCl saturated). A control experiment was carried out in 0.5 M Na_2SO_4 to verify electrochemical impacts other than Fe electrodeposition. Besides P-PI/GC, the MWCNTs/GC electrode was treated in the same way for Fe electrodeposition−electrochemical dissolution.

2.3. ORR Characterizations. The ORR properties were evaluated first with cyclic and then RRDE voltammetry in 0.5 M H_2SO_4. Before RRDE voltammograms were recorded, pretreatment was conducted on the Pt-ring electrode by repetitive potential sweep between 0 and 1.4 V until characteristic peaks of the clean Pt electrode appeared. During recording of the voltammograms, the Pt-ring electrode was kept at a constant potential of 1.2 V to measure the oxidation current of H_2O_2 produced on the disk electrode during the ORR.

2.4. X-ray Absorption Fine Structure (XAFS) Spectroscopy. Fe K-edge XAFS characterizations were carried out at BL14B2 of SPring-8, Japan. GC plates with the size of 30 × 10 × 1 mm were served as supports for P-PI or MWCNTs. In the same manner as section 2.2, one side (30 × 10 mm) of each GC plate was modified. After the electrochemical treatment described above, the GC plates were immersed in 0.5 M H_2SO_4 for storage to avoid exposure in air. For XAFS measurements, the GC plates were washed with Milli-Q water, dried in a glovebox under vacuum, and sealed in gas barrier bags (thickness of 70 μm) filled with Ar. The measurements were performed in the fluorescence yield mode using 19 elements of Ge solid-state detectors at grazing incidence geometry to gain the signal of Fe with a low concentration. XAFS spectra of the reference materials, including iron phthalocyanine (FePc), FeO, α-Fe_2O_3, Fe_3O_4, Fe foil, $FeF_3·3H_2O$, FeS_2, and $FeSO_4·7H_2O$, were recorded in the transmission mode. All of the spectra were obtained at room temperature. The XAFS data were analyzed using the Athena and Artemis software.[25] X-ray absorption near edge structure (XANES) was used for the chemical state analysis, while extended X-ray absorption fine

DOI: 10.1021/acs.langmuir.5b00310
Langmuir 2015, 31, 5529−5536

structure (EXAFS) was used to obtain the local structural information for each chemical component. Fe K-edge EXAFS signals $\chi(k)$ were extracted and Fourier-transformed over the k-space range of 2−8 Å^{-1}, using k^3 weight and a Hanning window.

3. RESULTS AND DISCUSSION

3.1. Influence of the Electrochemical Treatment on ORR. In comparison to the cyclic voltammogram (CV) recorded in Ar-saturated 0.5 M Na_2SO_4, the CV in the solution containing 0.1 M $FeSO_4$ exhibits a typical cathodic peak around −0.77 V corresponding to the reduction of Fe^{2+} to Fe^0 (see Figure S2 of the Supporting Information). During the electrodeposition, small bubbles are observed on the surface of P-PI/GC electrodes because of hydrogen evolution on the Fe electrodeposited.[26,27] The electrode surface is covered by a film with gray luster after electrodeposition. All of these facts demonstrate that Fe has been successfully electrodeposited. CVs for the ORR on P-PI/GC electrodes with and without the electrochemical treatment are shown in Figure 1, and it can

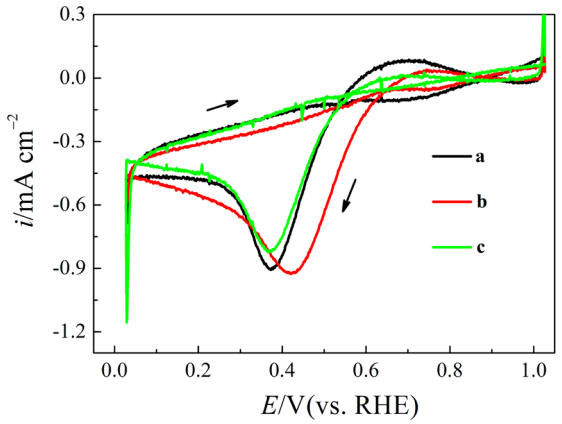

Figure 1. CVs recorded at different P-PI/GC electrodes (a, without treatment; b, with the electrochemical treatment in 0.5 M Na_2SO_4 containing 0.1 M $FeSO_4$; and c, with the electrochemical treatment in 0.5 M Na_2SO_4) in O_2-saturated 0.5 M H_2SO_4 (with background subtraction). Scan rate = 50 mV s^{-1}.

seen clearly that the peak potential is shifted in the positive direction by the electrochemical treatment in $FeSO_4$-containing 0.5 M Na_2SO_4 solution (curve b), while when the treatment is carried out in the solution without $FeSO_4$, no potential shift is obtained (curve c). Consequently, the Fe electrodeposition−electrochemical dissolution is responsible for the decrease of ORR overpotential.

The same electrochemical treatment was employed on the MWCNTs/GC electrode to ascertain whether nitrogen is essential for the formation of bondings responsible for the improved ORR activity, and the results are exhibited in Figure 2. The Fe electrodeposition−electrochemical dissolution causes no positive shift in the ORR peak potential. Therefore, it is suggested that nitrogen is vital for the introduction of active sites for ORR.

3.2. Local Structure Analysis of Fe Introduced by Electrochemical Methods. To elucidate the mechanism of enhanced ORR activity by the Fe electrodeposition−electrochemical dissolution, it is important to identify the chemical states of Fe. XPS, a common technique for elemental and chemical state characterizations, has been employed to obtain Fe 2p information, but unfortunately, the signals are too noisy

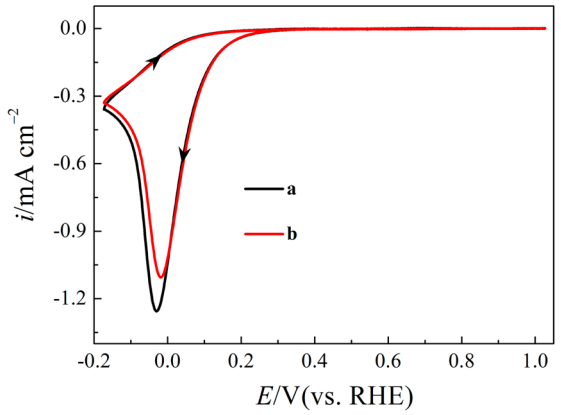

Figure 2. CVs obtained at different MWCNTs/GC electrodes (a, without treatment; b, with the electrochemical treatment in 0.5 M Na_2SO_4 containing 0.1 M $FeSO_4$) in O_2-saturated 0.5 M H_2SO_4 (with background subtraction). Scan rate = 50 mV s^{-1}.

because of the quite low Fe concentration. Although the N 1s spectrum is obtained for the P-PI with the treatment of Fe electrodeposition−electrochemical dissolution, there is no obvious difference from that without treatment (see Figure S1 of the Supporting Information), and it is quite difficult to define the presence of possible bondings between Fe and nitrogen. Accordingly, Fe K-edge XAFS in the fluorescence yield mode with the detection limit down to 10 ppm was used.

XANES spectra of P-PI/GC and MWCNTs/GC treated by the Fe electrodeposition−electrochemical dissolution are shown in Figure 3, together with reference compounds. The edge position of P-PI/GC and MWCNTs/GC is 7121 eV in this work. As seen, the edge position and profiles of treated P-PI/GC and MWCNTs/GC are similar to those of FePc (Fe^{2+}: D_{4h} symmetry) or Fe_3O_4 (Fe^{2+} + Fe^{3+}: Fe^{2+}, O_h; Fe^{3+}, O_h; and Fe^{3+}, T_d symmetries), indicating that Fe species introduced by

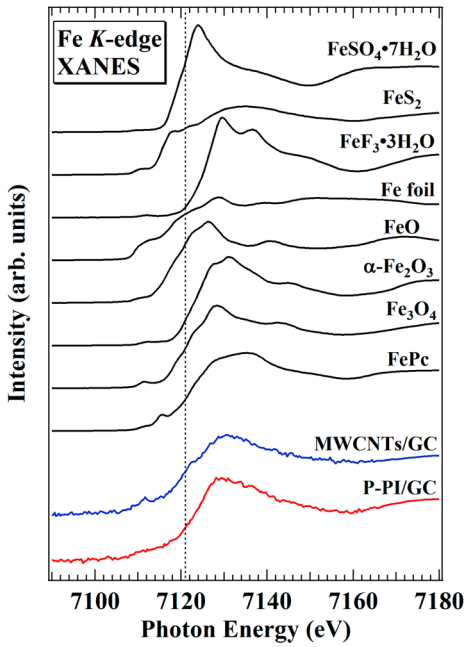

Figure 3. Fe K-edge XANES spectra of P-PI/GC and MWCNTs/GC with the electrochemical treatment in 0.5 M Na_2SO_4 containing 0.1 M $FeSO_4$. Spectra of reference samples are also shown for comparison.

DOI: 10.1021/acs.langmuir.5b00310
Langmuir 2015, 31, 5529−5536

the electrochemical treatment are in the oxidized states instead of the metallic state. Although Nafion and $FeSO_4$ are used during the electrode modification and electrochemical treatment, F- or S-containing components, such as FeF_3, FeS_2, and $FeSO_4$, seem to be absent in P-PI/GC and MWCNTs/GC because of the differences in edge position and profile. In the spectrum of MWCNTs/GC, a pre-edge peak at around 7112 eV is observed. This peak is assigned to the dipole-forbidden 1s → 3d transition and gains its intensity from the dipole-allowed transition in p−d hybridization, such as T_d symmetry.[28] Thus, Fe species with T_d symmetry may be formed in MWCNTs/GC. On the other hand, the pre-edge peak is less distinct in the P-PI/GC spectrum. Therefore, other types of Fe species may be formed in the P-PI/GC. The local structure of Fe is further discussed below by the EXAFS analysis.

As shown in Figure 4, there is a substantial difference in the Fourier transform (FT) EXAFS spectra of P-PI and MWCNTs/GC treated by the electrochemical method. Two peaks are dominant in the spectrum of the MWCNTs/GC, which is characteristic for Fe oxides, in particular, Fe_3O_4. Referring to the EXAFS analysis of Fe_3O_4,[29] the peak at around 1.5 Å corresponds to the first Fe−O bond and the peak between 2 and 3.5 Å is attributed to the Fe−Fe bond in the second sphere of Fe_3O_4. Because the MWCNTs are nitrogen-free, the possibility of a Fe−N bond for the peak at around 1.5 Å is ruled out. Metallic Fe can also be excluded because the peak position of the Fe−Fe bond in Fe foil is around 2.1 Å (see Figure S4 of the Supporting Information). Consequently, Fe species introduced to MWCNTs/GC are in the form of Fe oxides, which is consistent with the results of the XANES spectrum. In combination with CVs above, it can be concluded that Fe oxides introduced into the MWCNTs/GC electrode by the Fe electrodeposition−electrochemical dissolution are not active for ORR.

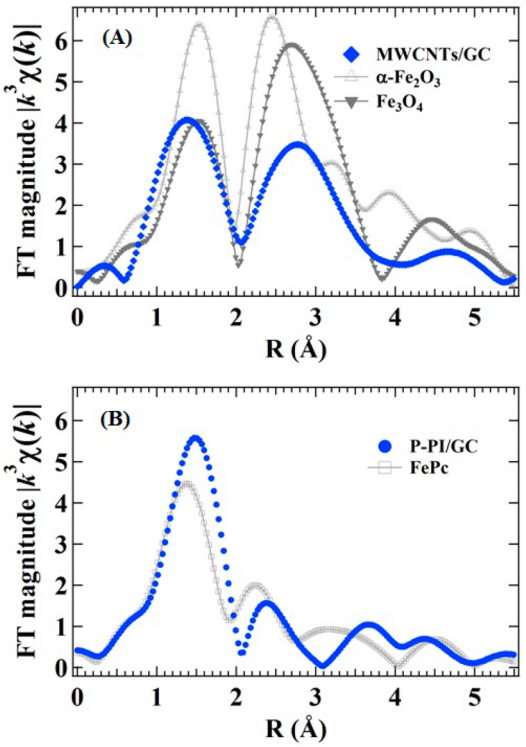

Figure 4. FT EXAFS spectra of (A) MWCNTs/GC and (B) P-PI/GC with the electrochemical treatment in 0.5 M Na_2SO_4 containing 0.1 M $FeSO_4$. The spectra of (A) α-Fe_2O_3 and Fe_3O_4 and (B) FePc are also displayed.

Only one peak at around 1.5 Å is observed on the FT EXAFS spectrum of the electrochemically treated P-PI/GC, which compares very well to that of FePc, and thus, the peak can be assigned possibly to the Fe−N bond. The absence of a distinct peak at larger distances indicates that a neighboring Fe−Fe bond does not exist, and it follows that Fe oxides or metallic Fe are not formed in the P-PI/GC. These observations strongly support that this peak originates from the Fe−N bond rather than the Fe−O bond, although the possibility of O−Fe−N centers present in compounds such as Fe salen cannot be ruled out. At the first scanning for Fe electrochemical dissolution (see Figure S3 of the Supporting Information), there is a local high concentration of Fe^{2+} in the vicinity of the P-PI/GC electrode, as proven by the large anodic current, which is favorable for the coordination. In the meanwhile, the present P-PI sample possesses 32.0% of pyridinic nitrogen, which is believed to preferably coordinate with metal ions for NDC materials,[10,14,30] and hence, the coordination of Fe with nitrogen is expected. Fe L-edge soft X-ray emission spectroscopy measurement of the treated P-PI also supports the existence of Fe−N_x (see Figure S5 of the Supporting Information). Therefore, different from MWCNTs/GC, Fe−N_x sites are present in the treated P-PI/GC with improved catalytic activity.

To further analyze the FT EXAFS spectrum of the P-PI/GC, curve fitting was carried out using a single nitrogen atomic shell. The obtained parameters are listed in Table 1, and the fitted curves are shown in Figure S4 of the Supporting Information. The amplitude reduction factor (S_0^2) is calculated to be 0.955 when the coordination number (N') of FePc is fixed to be 4. The estimated N' of the P-PI/GC is 5.3 ± 1.3, which is in good agreement with the reported Fe−N_x structures active for ORR, such as Fe−N_4, N−Fe−N_{2+2}, N−Fe−N_4, and Fe−N_{2+2+2}.[31−34] Furthermore, the distance for the Fe−N bond in the treated P-PI/GC is estimated to be 2.04 ± 0.02 Å, which is slightly larger than that of FePc. In combination with the higher values of N' than 4, the Fe−N bond in the P-PI/GC is probably distorted and/or forms a square-pyramidal-like structure, where Fe atoms locate above the basal plane.[35]

3.3. Kinetic Analysis on ORR. Because better ORR performance was obtained on the P-PI/GC electrode treated with the Fe electrodeposition−electrochemical dissolution, RRDE voltammetry was further conducted, and the results

Table 1. Coordination Number (N'), Distance between the Nearest Neighbors (R), Debye−Waller Factor (σ^2), and Amplitude Reduction Factor (S_0^2) of FePc and P-PI/GC with the Electrochemical Treatment in 0.5 M Na_2SO_4 Containing 0.1 M $FeSO_4$ That Are Estimated from the Fe K-Edge EXAFS Analysis

sample	bond type	N'	R (Å)	σ^2 (×10^{-3}, Å^2)	S_0^2
FePc	Fe−N	4	1.93 ± 0.07	8.5 ± 10.1	0.955
P-PI/GC	Fe−N	5.3 ± 1.3	2.04 ± 0.02	9.4 ± 4.2	0.955

DOI: 10.1021/acs.langmuir.5b00310
Langmuir 2015, 31, 5529−5536

are presented in Figure 5. Better ORR performance of the P-PI/GC electrode (curve b) than that of the bare electrode

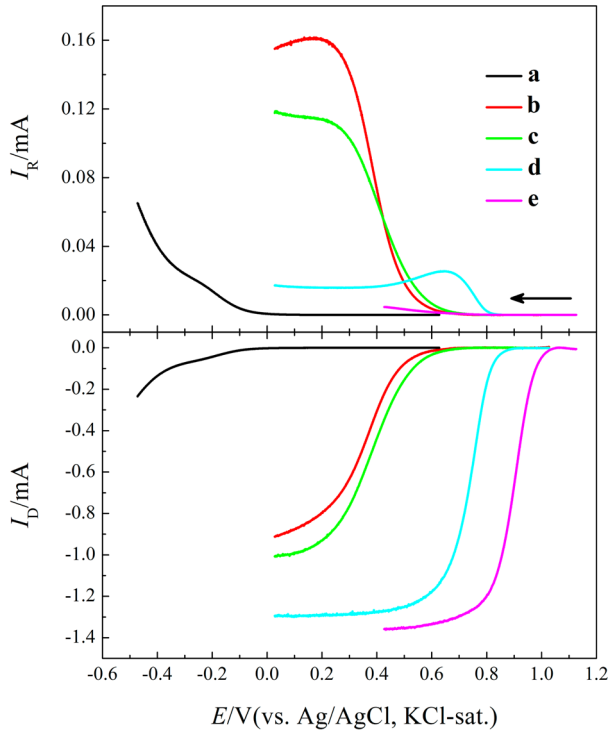

Figure 5. Comparison of RRDE voltammograms on different electrodes (a, bare GC electrode; b, P-PI/GC electrode without treatment; c, P-PI/GC electrode with the electrochemical treatment in 0.5 M Na_2SO_4 containing 0.1 M $FeSO_4$; d, Fe-containing P-PI [prepared via pyrolysis in the presence of $Fe(C_5H_7O_2)_3$] modified GC electrode; and e, Pt−C/GC electrode) in O_2-saturated 0.5 M H_2SO_4 (with background subtraction). Scan rate = 5 mV s^{-1}, and rotation rate = 1600 rpm.

(curve a) is closely related to the activity of the nitrogen−carbon bond and higher surface area. With the electrochemical treatment (curve c), the onset potential, defined as a potential at which the disk current density reaches −10 μA cm^{-2}, has been altered from 0.68 to 0.71 V and the half-wave potential is also shifted positively (from 0.36 to 0.38 V). Besides the positive shift in both onset and half-wave potential, the disk current is increased and the ring current decreases in the meanwhile. All of these facts demonstrate that the ORR performance is improved by the Fe electrodeposition−electrochemical dissolution. Unfortunately, the ORR activity of the treated P-PI/GC electrode is still inferior to that of Fe-containing P-PI prepared via the multi-step pyrolysis in the presence of $Fe(C_5H_7O_2)_3$ (curve d) and commercial Pt/C (46 wt % Pt) (curve e) modified GC electrodes, in which the loading density of individual catalysts is the same (200 μg cm^{-2}). In combination with the analysis of XAFS results, conclusions can be drawn that the catalytic activity of Fe−N_x sites introduced by the electrochemical treatment is higher than that of nitrogen−carbon structures in P-PI and lower than that of active sites in pyrolyzed Fe-containing P-PI. However, there is a mixture of different Fe species in the Fe-containing P-PI prepared by pyrolysis,[22] and it is difficult to define the exact sites active for ORR. Anyway, Fe−N_x introduced into the present P-PI by the electrochemical treatment is a kind of active site for ORR.

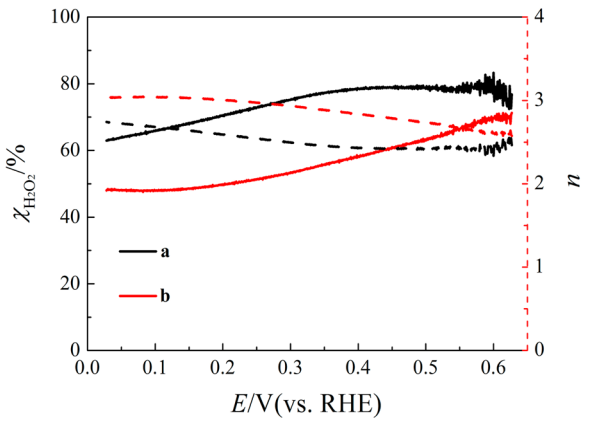

Figure 6. Potential dependence of $\chi_{H_2O_2}$ and n at different P-PI/GC electrodes (a, without treatment; b, with the electrochemical treatment in 0.5 M Na_2SO_4 containing 0.1 M $FeSO_4$).

Figure 6 shows the potential dependence of $\chi_{H_2O_2}$ and n at different P-PI/GC electrodes calculated according to eqs. 1 and 2, in which I_D and I_R represent the disk and ring currents, respectively, and N, collection efficiency, has a value of 0.37 in this case.

$$\chi_{H_2O_2} = 100(2I_R/N)/(I_D + I_R/N) \quad (1)$$

$$n = 4I_D/(I_D + I_R/N) \quad (2)$$

For the P-PI/GC electrode without treatment, $\chi_{H_2O_2}$ is around 80% at 0.6 V and decreases as the potential becomes more negative; however, its value is still larger than 60% at the potential of 0.05 V. Correspondingly, n increases from 2.4 at 0.6 V to 2.8 at 0.05 V. These results suggest the coexistence of two- and four-electron ORR and, in addition, that the two-electron process is predominant. On the other hand, a decrease in $\chi_{H_2O_2}$ and an increase in n are observed on the P-PI/GC electrode treated by the Fe electrodeposition−electrochemical dissolution, indicating that four-electron ORR is enhanced.

As stated in the Introduction, it is quite necessary to obtain the individual rate constants of ORR (k_1, k_2, and k_3) to identify the pathway. The model proposed by Damjanovic et al. (Scheme 1) is selected,[21] and the values of k at different potentials are obtained by the following equations:[36]

$$k_1 = Z_1S_2(I_1N - 1)/(I_1N + 1) \quad (3)$$

$$k_2 = 2Z_1S_2/(I_1N + 1) \quad (4)$$

$$k_3 = Z_2NS_1/(I_1N + 1) \quad (5)$$

where $Z_1 = 0.62D_{O_2}^{2/3}\upsilon^{-1/6}$ and $Z_2 = 0.62D_{H_2O_2}^{2/3}\upsilon^{-1/6}$. I_1 and S_1 are the intercept and slope of $-I_D/I_R$ versus $\omega^{-1/2}$ plots, respectively, and ω is the angular frequency of rotation. S_2 is the slope of $I_{DL}/(I_{DL} - I_D)$ versus $\omega^{-1/2}$ plots, and I_{DL} stands for the disk-limiting current. The values of D_{O_2} (diffusion coefficient of O_2), $D_{H_2O_2}$ (diffusion coefficient of H_2O_2), and υ (kinematic viscosity of 0.5 M H_2SO_4) are cited as 1.4×10^{-5}, 6.8×10^{-6}, and 0.01 cm^2 s^{-1}, respectively.[37]

DOI: 10.1021/acs.langmuir.5b00310
Langmuir 2015, 31, 5529−5536

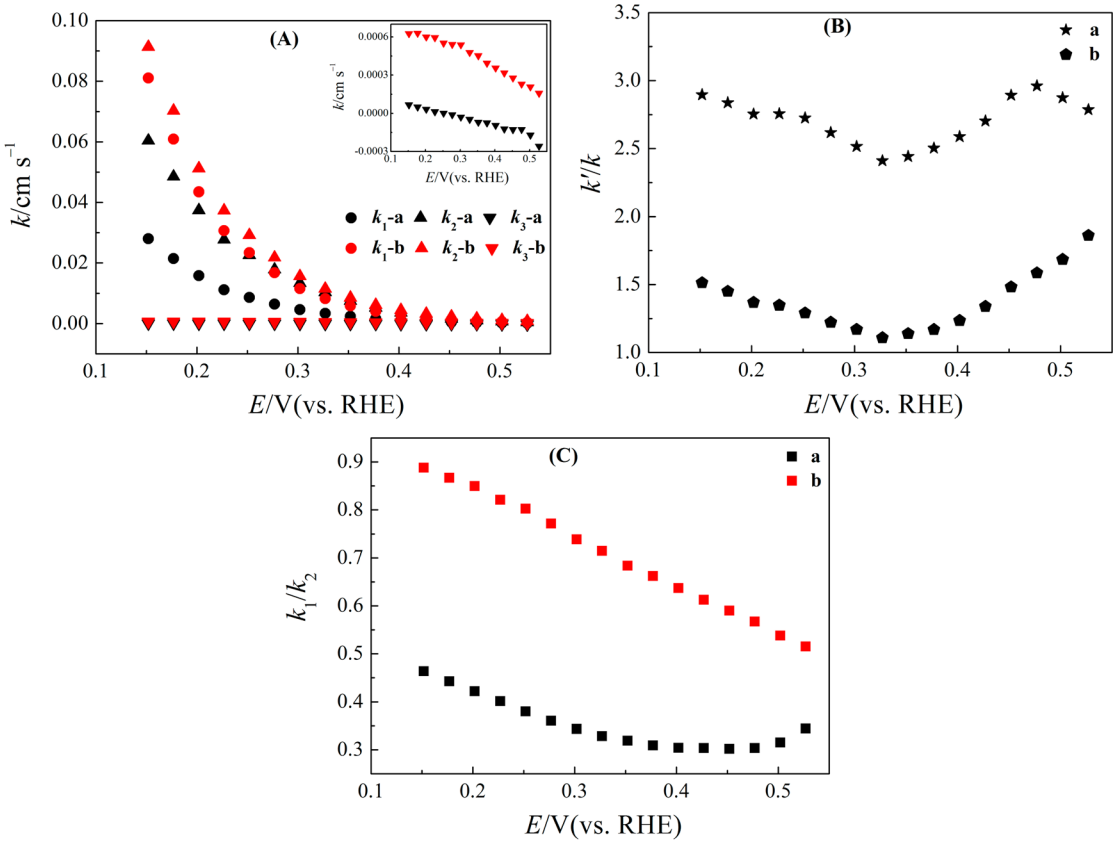

Figure 7. Dependency of (A) k and (C) k_1/k_2 on potential at different P-PI/GC electrodes (a, without treatment; b, with the electrochemical treatment in 0.5 M Na_2SO_4 containing 0.1 M $FeSO_4$). The inset of panel A shows the enlarged plots on k_3. (B) Changes in (a) k_1 and (b) k_2 induced by the electrochemical treatment. The symbols of k and k' represent rate constants before and after the treatment, respectively.

The potential dependence of k at the P-PI/GC electrode with the electrochemical treatment is given in Figure 7A, in which the result obtained at the untreated electrode is also shown for comparison. On the untreated P-PI/GC electrode, $k_2 > k_1 \gg k_3 \approx 0$, suggesting that the pathway of ORR is in the parallel pattern and O_2 molecules are predominantly reduced to H_2O_2. All of the rate constants at the treated P-PI electrode are increased in comparison to those at the untreated electrode. The values of k_1 and k_2 are comparable, but the k_3 values are much smaller than them, i.e., $k_1 \sim k_2 \gg k_3$. In comparison to k_2, the increase in k_1 is much larger (Figure 7B), and accordingly, the ratios of k_1/k_2 are improved (Figure 7C). In combination with the results from XAFS measurements, it is obvious that Fe−N_x plays an important role in the enhancement of direct four-electron reduction of O_2, being in good accordance with the view that Fe−N_x sites are active for four-electron ORR.[15,31,34] It is noted here that the values of k_1/k_2 after the Fe−N_x introduction are still less than unity, while those of 5.5−8.3 are obtained on the Fe-containing P-PI prepared via pyrolysis in the presence of $Fe(C_5H_7O_2)_3$.[38] Besides the differences in microstructure, specific surface area, contents of diverse elements, and Fe species between the Fe-containing and Fe-free P-PI samples,[22] the smaller k_1/k_2 values at the latter catalyst treated by the Fe electrodeposition−electrochemical dissolution may be related to the limited amount of Fe−N_x sites. The quantity of Fe electrodeposited is far larger than that used for bonding with nitrogen, and the number of Fe−N_x sites could be restricted by pyridinic nitrogen.[39] Larger enhancement in ORR performance by the Fe electrodeposition−electrochemical dissolution might be expected for NDC materials with a higher content of pyridinic nitrogen.

Besides 200 μg cm^{-2}, the same experiments were performed on the P-PI/GC electrodes with loading densities of 100 and 50 μg cm^{-2}. The values of k_3 are still close to zero, and those of k_1 and k_2 are decreased with lowering the loading (see Figures S5 and S6 of the Supporting Information). The ratios of k_1/k_2 are raised on all of the electrodes by the electrodeposition−electrochemical dissolution of Fe, and the role of Fe−N_x in the enhancement of direct four-electron reduction of O_2 is verified.

4. CONCLUSION

The introduction of Fe species into P-PI has been achieved by the treatment of Fe electrodeposition−electrochemical dissolution at room temperature. After the electrochemical treatment, the overpotential of ORR on the P-PI is decreased. Further kinetic analysis demonstrates the coexistence of two- and four-electron ORR in parallel pattern on the P-PI. The Fe introduction leads to a larger increase in k_1 than in k_2, and accordingly, smaller $\chi_{H_2O_2}$ and larger n are observed. This enhancement in ORR kinetics is closely related to the presence of Fe−N_x sites, which are believed to be active for four-electron reduction of O_2. Unfortunately, the ratios of k_1/k_2 are still less than unity even after the introduction of Fe−N_x, which may be due to the low density of such sites limited by the number of pyridinic nitrogen in the P-PI. NDC materials with a higher content of pyridinic nitrogen will be concerned in the future.

DOI: 10.1021/acs.langmuir.5b00310
Langmuir 2015, 31, 5529−5536

■ ASSOCIATED CONTENT

Supporting Information

XPS N 1s spectra (Figure S1), additional CVs (Figures S2 and S3), Fe L soft X-ray emission spectra (Figure S4), curve fitting of FT EXAFS spectra (Figure S5), and ORR rate constants on P-PI/GC electrodes with loading densities of 100 and 50 μg cm^{-2} (Figures S6 and S7). The Supporting Information is available free of charge on the ACS Publications website at DOI: 10.1021/acs.langmuir.5b00310.

■ AUTHOR INFORMATION

Corresponding Author

*E-mail: ohsaka@echem.titech.ac.jp.

Notes

The authors declare no competing financial interest.

■ ACKNOWLEDGMENTS

This work was financially supported by the New Energy and Industrial Technology Development Organization (NEDO), Japan. The synchrotron radiation experiments were performed at SPring-8 with the approval of the Japan Synchrotron Radiation Research Institute (JASRI) (Proposal 2014A1752) and jointly by the Synchrotron Radiation Research Organization and the University of Tokyo (Proposal 2014A7403). The authors thank Prof. T. Fuchigami and Dr. A. Muthukrishnan for helpful discussion.

■ REFERENCES

(1) You, C.; Zen, X.; Qiao, X.; Liu, F.; Shu, T.; Du, L.; Zeng, J.; Liao, S. Fog-like fluffy structured N-doped carbon with a superior oxygen reduction reaction performance to a commercial Pt/C catalyst. *Nanoscale* **2015**, *7*, 3780−3785.

(2) Yan, J.; Meng, H.; Xie, F. Y.; Yuan, X. L.; Yu, W. D.; Lin, W. R.; Ouyang, W. P.; Yuan, D. S. Metal free nitrogen doped hollow mesoporous graphene-analogous spheres as effective electrocatalyst for oxygen reduction reaction. *J. Power Sources* **2014**, *245*, 772−778.

(3) Gong, K. P.; Du, F.; Xia, Z. H.; Durstock, M.; Dai, L. M. Nitrogen-doped carbon nanotube arrays with high electrocatalytic activity for oxygen reduction. *Science* **2009**, *323*, 760−764.

(4) Liu, R. L.; Wu, D. Q.; Feng, X. L.; Mullen, K. Nitrogen-doped ordered mesoporous graphitic arrays with high electrocatalytic activity for oxygen reduction. *Angew. Chem., Int. Ed.* **2010**, *49*, 2565−2569.

(5) Wei, W.; Liang, H. W.; Parvez, K.; Zhuang, X. D.; Feng, X. L.; Mullen, K. Nitrogen-doped carbon nanosheets with size-defined mesopores as highly efficient metal-free catalyst for the oxygen reduction reaction. *Angew. Chem., Int. Ed.* **2014**, *53*, 1570−1574.

(6) Li, Y. G.; Zhou, W.; Wang, H. L.; Xie, L. M.; Liang, Y. Y.; Wei, F.; Idrobo, J. C.; Pennycook, S. J.; Dai, H. J. An oxygen reduction electrocatalyst based on carbon nanotube−graphene complexes. *Nat. Nanotechnol.* **2012**, *7*, 394−400.

(7) Ganesan, S.; Leonard, N.; Barton, S. C. Impact of transition metal on nitrogen retention and activity of iron−nitrogen−carbon oxygen reduction catalysts. *Phys. Chem. Chem. Phys.* **2014**, *16*, 4576−4585.

(8) Wu, G.; More, K. L.; Johnston, C. M.; Zelenay, P. High-performance electrocatalysts for oxygen reduction derived from polyaniline, iron, and cobalt. *Science* **2011**, *332*, 443−447.

(9) Liu, G.; Li, X. G.; Ganesan, P.; Popov, B. N. Development of non-precious metal oxygen-reduction catalysts for PEM fuel cells based on N-doped ordered porous carbon. *Appl. Catal., B* **2009**, *93*, 156−165.

(10) Parvez, K.; Yang, S. B.; Hernandez, Y.; Winter, A.; Turchanin, A.; Feng, X. L.; Mullen, K. Nitrogen-doped graphene and its iron-based composite as efficient electrocatalysts for oxygen reduction reaction. *ACS Nano* **2012**, *6*, 9541−9550.

(11) Sahraie, N. R.; Paraknowitsch, J. P.; Goebel, C.; Thomas, A.; Strasser, P. Noble-metal-free electrocatalysts with enhanced ORR performance by task-specific functionalization of carbon using ionic liquid precursor systems. *J. Am. Chem. Soc.* **2014**, *136*, 14486−14497.

(12) Yu, D. S.; Zhang, Q.; Dai, L. M. Highly efficient metal-free growth of nitrogen-doped single-walled carbon nanotubes on plasma-etched substrates for oxygen reduction. *J. Am. Chem. Soc.* **2010**, *132*, 15127−15129.

(13) Olson, T. S.; Pylypenko, S.; Fulghum, J. E.; Atanassov, P. Bifunctional oxygen reduction reaction mechanism on non-platinum catalysts derived from pyrolyzed porphyrins. *J. Electrochem. Soc.* **2010**, *157*, B54−B63.

(14) Lefevre, M.; Dodelet, J. P.; Bertrand, P. Molecular oxygen reduction in PEM fuel cells: Evidence for the simultaneous presence of two active sites in Fe-based catalysts. *J. Phys. Chem. B* **2002**, *106*, 8705−8713.

(15) Lin, L.; Zhu, Q.; Xu, A. W. Noble-metal-free Fe−N/C catalyst for highly efficient oxygen reduction reaction under both alkaline and acidic conditions. *J. Am. Chem. Soc.* **2014**, *136*, 11027−11033.

(16) Nallathambi, V.; Lee, J. W.; Kumaraguru, S. P.; Wu, G.; Popov, B. N. Development of high performance carbon composite catalyst for oxygen reduction reaction in PEM proton exchange membrane fuel cells. *J. Power Sources* **2008**, *183*, 34−42.

(17) Kobayashi, M.; Niwa, H.; Saito, M.; Harada, Y.; Oshima, M.; Ofuchi, H.; Terakura, K.; Ikeda, T.; Koshigoe, Y.; Ozaki, J.; Miyata, S. Indirect contribution of transition metal towards oxygen reduction reaction activity in iron phthalocyanine-based carbon catalysts for polymer electrolyte fuel cells. *Electrochim. Acta* **2012**, *74*, 254−259.

(18) Wang, P.; Ma, Z. Y.; Zhao, Z. C.; Ha, L. X. Oxygen reduction on the electrocatalysts based on pyrolyzed non-noble metal/poly-*o*-phenylenediamine/carbon black composites: New insight into the active sites. *J. Electroanal. Chem.* **2007**, *611*, 87−95.

(19) Geng, D. S.; Chen, Y.; Chen, Y. G.; Li, Y. L.; Li, R. Y.; Sun, X. L.; Ye, S. Y.; Knights, S. High oxygen-reduction activity and durability of nitrogen-doped graphene. *Energy Environ. Sci.* **2011**, *4*, 760−764.

(20) Choi, C. H.; Chung, M. W.; Kwon, H. C.; Chung, J. H.; Woo, S. I. Nitrogen-doped graphene/carbon nanotube self-assembly for efficient oxygen reduction reaction in acid media. *Appl. Catal., B* **2014**, *144*, 760−766.

(21) Damjanov, A.; Genshaw, M. A.; Bockris, J. O. Distinction between intermediates produced in main and side electrodic reaction. *J. Chem. Phys.* **1966**, *45*, 4057−4059.

(22) Nabae, Y.; Kuang, Y. B.; Chokai, M.; Ichihara, T.; Isoda, A.; Hayakawa, T.; Aoki, T. High performance Pt-free cathode catalysts for polymer electrolyte membrane fuel cells prepared from widely available chemicals. *J. Mater. Chem. A* **2014**, *2*, 11561−11564.

(23) Diaz, S. L.; Calderon, J. A.; Barcia, O. E.; Mattos, O. R. Electrodeposition of iron in sulphate solutions. *Electrochim. Acta* **2008**, *53*, 7426−7435.

(24) Grujicic, D.; Pesic, B. Iron nucleation mechanisms on vitreous carbon during electrodeposition from sulfate and chloride solutions. *Electrochim. Acta* **2005**, *50*, 4405−4418.

(25) Ravel, B.; Newville, M. ATHENA, ARTEMIS, HEPHAESTUS: Data analysis for X-ray absorption spectroscopy using IFEFFIT. *J. Synchrotron Radiat.* **2005**, *12*, 537−541.

(26) Meguro, S.; Sasaki, T.; Katagiri, H.; Habazaki, H.; Kawashima, A.; Sakaki, T.; Asami, K.; Hashimoto, K. Electrodeposited Ni−Fe−C cathodes for hydrogen evolution. *J. Electrochem. Soc.* **2000**, *147*, 3003−3009.

(27) Zarpellon, J.; Jurca, H. F.; Klein, J. J.; Schreiner, W. H.; Mattoso, N.; Mosca, D. H. Electrodeposition of Fe thin films on Si(111) surfaces in the presence of sodium saccharin. *Electrochim. Acta* **2007**, *53*, 2002−2008.

(28) Roe, A. L.; Schneider, D. J.; Mayer, R. J.; Pyrz, J. W.; Widom, J.; Que, L. X-ray absorption spectroscopy of iron−tyrosinate proteins. *J. Am. Chem. Soc.* **1984**, *106*, 1676−1681.

(29) Subias, G.; Garcia, J.; Blasco, J. EXAFS spectroscopic analysis of the Verwey transition in Fe_3O_4. *Phys. Rev. B* **2005**, *71*, 155103.

DOI: 10.1021/acs.langmuir.5b00310
Langmuir 2015, 31, 5529−5536

(30) Byon, H. R.; Suntivich, J.; Shao-Horn, Y. Graphene-based non-noble-metal catalysts for oxygen reduction reaction in acid. *Chem. Mater.* **2011**, *23*, 3421−3428.
(31) Kramm, U. I.; Lefevre, M.; Larouche, N.; Schmeisser, D.; Dodelet, J.-P. Correlations between mass activity and physicochemical properties of Fe/N/C catalysts for the ORR in PEM fuel cell via Fe-57 Mossbauer spectroscopy and other techniques. *J. Am. Chem. Soc.* **2014**, *136*, 978−985.
(32) Tylus, U.; Jia, Q.; Strickland, K.; Ramaswamy, N.; Serov, A.; Atanassov, P.; Mukerjee, S. Elucidating oxygen reduction active sites in pyrolyzed metal−nitrogen coordinated non-precious-metal electrocatalyst systems. *J. Phys. Chem. C* **2014**, *118*, 8999−9008.
(33) Cao, R.; Thapa, R.; Kim, H.; Xu, X.; Kim, M. G.; Li, Q.; Park, N.; Liu, M.; Cho, J. Promotion of oxygen reduction by a bio-inspired tethered iron phthalocyanine carbon nanotube-based catalyst. *Nat. Commun.* **2013**, 2076.
(34) Ferrandon, M.; Kropf, A. J.; Myers, D. J.; Artyushkova, K.; Kramm, U.; Bogdanoff, P.; Wu, G.; Johnston, C. M.; Zelenay, P. Multitechnique characterization of a polyaniline−iron−carbon oxygen reduction catalyst. *J. Phys. Chem. C* **2012**, *116*, 16001−16013.
(35) Arcovito, A.; Benfatto, M.; D'Angelo, P.; Della Longa, S. Hemeproteins: Recent advances in quantitative XANES analysis. *AIP Conf. Proc.* **2007**, *882*, 306−310.
(36) Hsueh, K. L.; Chin, D. T.; Srinivasan, S. Electrode kinetics of oxygen reduction: A theoretical and experimental analysis of the rotating ring-disc electrode method. *J. Electroanal. Chem.* **1983**, *153*, 79−95.
(37) Alonsovante, N.; Tributsch, H.; Solorzaferia, O. Kinetics studies of oxygen reduction in acid medium on novel semiconducting transtion metal chalcogenides. *Electrochim. Acta* **1995**, *40*, 567−576.
(38) Muthukrishnan, A.; Nabae, Y.; Hayakawa, T.; Okajima, T.; Ohsaka, T. Fe-containing polyimide-based high-performance ORR catalysts in acidic medium: A kinetic approach to study the durability of catalysts. *Catal. Sci. Technol.* **2015**, *5*, 475−483.
(39) Faubert, G.; Cote, R.; Dodelet, J. P.; Lefevre, M.; Bertrand, P. Oxygen reduction catalysts for polymer electrolyte fuel cells from the pyrolysis of Fe^{II} acetate adsorbed 3,4,9,10-perylenetetracarboxylic dianhydride. *Electrochim. Acta* **1999**, *44*, 2589−2603.

DOI: 10.1021/acs.langmuir.5b00310
Langmuir 2015, 31, 5529−5536